Finite Deformation Field near the Tip of a Blatz-Ko Wedge Bonded to a Rigid Substrate

Chung-Yuen Hui^{1,2,#}, Bangguo Zhu^{1,#,*}, and Matteo Ciccotti³

- # These two authors contributed equally to this work
- * Corresponding Author, email: <u>bz347@cornell.edu</u>

Abstract

Sharp corners or wedges are common in everyday structures. Depending on the internal angle θ_0 of the wedge, severe stress concentration can occur. Linear elasticity predicts that when an incompressible elastic wedge is bonded to a rigid substrate and subjected to plane strain deformation, the stresses at the wedge tip has a power law singularity if $\theta_0 > 45^0$. For some θ_0 and for compressible wedges, the stresses are not only singular but oscillate infinitely rapidly. Here we show that these results are no longer true if large deformation is taken into consideration. Specifically, we determine the asymptotic fields near a tip of a Blatz-Ko wedge and found that the stress field has no power singularity for $\theta_0 \leq 90^{\circ}$. Furthermore, the power law singularity of the stress field differs from those predicted by linear elasticity and there are no oscillations. For sufficiently low compressibility, it is possible to obtain higher order terms of the asymptotic series – analogous to William's expansion in linear theory. Our asymptotic results are validated by finite element (FE) calculations. We also studied the wedge tip field for the borderline case of a 90° wedge. For this case, the stress singularity is found to be at most logarithmic.

Keywords: Finite strain, Hyperelasticity, Compressible, Wedge, Asymptotic analysis, Finite element analysis

¹Field of Theoretical and Applied Mechanics, Dept. of Mechanical and Aerospace Engineering, Cornell University, Ithaca, NY 14853;

²Global Station for Soft Matter, Global Institution for Collaborative Research and Education (GI-CoRE), Hokkaido University, Sapporo 001-0021, Japan;

³Sciences et Ingénierie de la Matière Molle, CNRS UMR 7615, École Supérieure de Physique et de Chimie Industrielles de la Ville de Paris (ESPCI), ParisTech, PSL Research Univeristy, 10 rue Vauquelin, F-75231 Paris cedex 05, France

1. Introduction

Wedge shaped corners are ubiquitous in structures. For example, the use of patches bonded with structural adhesives is increasingly widespread in applications such as aircrafts, cars and other transport related applications. However, adhesively bonded patches have problems of stress concentration at the corners where crack initiation is prone to occur leading to the debonding of the patch. Such stress concentration can be reduced by tapering the surfaces of the patch, but tapering the adhesive is also an option (Marques and da Silva, 2008). In nature, small animals can achieve strong and robust adhesion with small patches such as the suction cups of octopus (Tramacere et al., 2014), the sticky fibrils of mussels (Ornes, 2013), vine tree and gecko feet (Arzt, Gorb and Spolenak, 2003). This strategy employed by nature has motivated the development of bioinspired structured adhesive surfaces (Gorb et al., 2006; Kim and Sitti, 2006; Jagota and Hui, 2011) to control adhesion and friction. These surfaces are typically made of an array of soft elastomeric fibers with shear modulus on the order of I MPa. Adhesion is typically measured against a rigid smooth surface such as glass. Experimentally and theoretically, it has been found that the shape of fiber tip can significantly affect contact and adhesion (del Campo, Greiner and Arzt, 2007; Spuskanyuk et al., 2008). Using finite element (FE) simulations based on linear elasticity and a cohesive zone model for debonding, Aksak, Sahin and Sitti, (2014) have found that wedge shape fiber tips (see Fig.1 insert) with an internal angle of $\theta_0 = 45^{\circ}$ optimize the pull-off stress per unit contact area of a single fiber¹.

Motivated by these applications, we study the generic problem in Figure 1 where a wedge in an elastic solid is bonded to a rigid substrate; depending on the internal angle θ_0 of the wedge, severe stress concentration is known to occur. Williams, (1952) was the first to study the stress singularity near a wedge tip in a linear isotropic elastic solid. He studied various sets of boundary conditions (BC) on the radial edges of a wedge in thin elastic plates under extension. William's ideas were later extended to wedges between dissimilar linear elastic materials, including anisotropic solid wedges (David B. Bogy, 1968; Hein and Erdogan, 1971; Dempsey and Sinclair, 1979). The main goal of these papers is to characterize the singular deformation and stress fields near the tip of elastic wedges. The use of these asymptotic fields to predict failure in applications can be found in Dunn et al. (Dunn et al., 1997; Dunn, Suwito and Cunningham, 1997, Leguillon, 2002). The idea is that these wedge singular fields fully characterize the stress and strain state

¹ There are other geometrical factors such as the aspect ratio of the fiber which control the optimal pull-off force.

near the wedge tip, hence their amplitude can be used as a loading parameter to determine crack initiation.

Here we note that all the above works are based on linearized theory of elasticity where both the kinematics and material behavior are linear. As a result, they generally work for hard and stiff solids. For soft materials such as adhesives and elastomers, the deformation near the wedge tip can be sufficiently large to violate the small strain assumption. Because of this, it is expected that there can be significant differences between the prediction of small strain and large deformation theory. For crack problems, these differences have been studied by Knowles and Steinberg (Knowles and Sternberg, 1973, 1974; J. K. Knowles and Sternberg, 1983), Stephenson (1982), Geubelle and Knauss (Geubelle, 1994a, 1994b, 1994c) and Gao (Gao, 1990). The finite strain crack tip fields exhibit characteristics that are drastically different from those of the linear elastic fracture mechanics solution, see (Long and Hui, 2015) for a detailed review. On the other hand, there are much fewer works on the behavior of the stress field near the tip of hyper-elastic wedges. Most of these works focus on homogeneous hyper-elastic solids (Mansouri et al., 2016). However, in many applications, such as those mentioned above, the wedge is bonded to very stiff substrates. This motivates us to consider the stress and deformation field near the tip of a hyper-elastic wedge (see Figure 1) that is bonded to a rigid substrate.

We consider plane strain deformation. The wedge in this work is a compressible hyperelastic solid proposed by (Blatz and Ko, 1962). This material model was used by (Lengyel, Long and Schiavone, 2014) to study the asymptotic behavior of an interface crack between a compressible hyper-elastic solid and a rigid substrate which corresponds to $\theta_0 = \pi$. Here we study the existence of singular fields near the wedge tip and, if they exist, how they depend on the wedge angle. These asymptotic solutions are validated by FE simulations.

The plan of this paper is as follows. In section 2 we review linear wedge asymptotic theory that is relevant to this work. In section 3 we introduce the finite strain model for the wedge problem. The asymptotic solution for $\pi > \theta_0 > \pi/2$ is given in section 4. In contrast to linear theory, where the transition between singular and non-singular tip solution occurs at $\theta_0 \approx \pi/4$ for solids with low compressibility, we found that there is no power-law singular solution for $\theta_0 \leq \pi/2$. In section 5, we check our asymptotic solution against FE simulations. In section 6, we study the transition case where $\theta_0 = \pi/2$. Summary and discussion are given in section 7.

2. Linearized theory of wedge tip fields (LTW)

To gain perspective, we summarize results based on linearized theory of elasticity that are relevant to this study. Williams, (1952) was the first to study the stress singularity near a wedge tip in a linear isotropic elastic solid. His studied various set of boundary conditions (BC) on the radial edges of a wedge in thin plates under extension. The BC that is relevant to this work is a clamped/free boundary. The clamped edge represents the rigid substrate in our problem (see Fig.1 for geometry). We note here that William's solution is for plane stress deformation. However, the solution of plane strain problems can be readily obtained from the plane stress solution by a simple transformation of elastic constants (Muskhelishvili, 1977). The results below are modified for plane strain deformation.

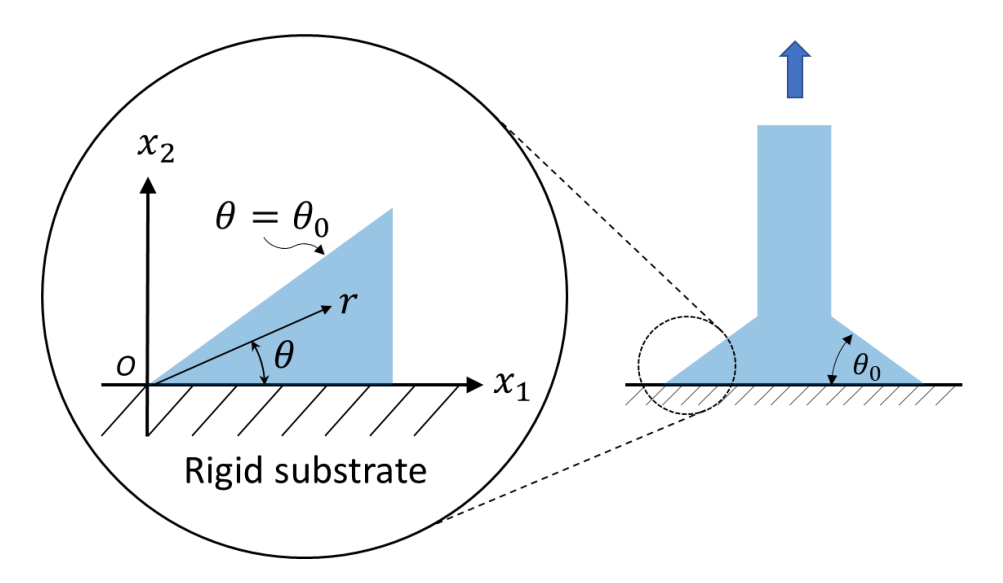


Figure 1: Figure inside circle shows local geometry of wedge for asymptotic analysis in the undeformed reference configuration. The lower edge of the wedge $\theta=0$ is bonded to the rigid substrate. Its edge at $\theta=\theta_0$ is traction free. We consider plane strain deformation where the out of plane displacement is identically zero and the fields are independent of x_3 . The out of plane coordinate x_3 is not shown. Geometry in the simulation of (Aksak, Sahin and Sitti, 2014) is shown on the right.

Williams, (1952) showed that the in-plane asymptotic stress field $\tau_{\alpha\omega}$, with respect to a polar coordinate system (r,θ) with origin at the wedge tip, has the form

$$\tau_{\alpha\alpha} = r^{m-1} \hat{\tau}_{\alpha\alpha} (\theta, \theta_0, \nu, A_1, A_2), \qquad r \to 0$$
 (1)

where A_1 and A_2 are loading parameters that controls the intensity of the stress field, ν is the Poisson's ratio of the elastic wedge and $\hat{\tau}_{\alpha\omega}$ are linear homogeneous functions of A_1 and A_2 . The parameters A_1 and A_2 cannot be determined from asymptotic analysis; they depend on the geometry of the structure and the manner of loading. In (1), m is the *singularity index* which can be complex. Typically, one requires that the real part of m to be greater than 0 so that the displacement field is bounded. Here we note the following:

• m is a function of the wedge angle θ_0 and the Poisson's ratio ν . Specifically, the relation between m and θ_0 for plane strain deformation is given by the transcendental equation:

$$m^{2} \sin^{2} \theta_{0} - 4(1-\nu)^{2} + (3-4\nu)\sin^{2}(m\theta_{0}) = 0.$$
 (2)

Note that the singularity index depends only on the Poisson's ratio and the wedge angle and is otherwise independent of material properties such as the shear modulus.

• m can be a complex number for some wedge angles, i.e., $m = m_1 + im_2$ where $i = \sqrt{-1}$. For this case, the stress can be obtained by taking the real or imaginary part of (1). Since

$$r^{m-1} = r^{m_1-1} \Big[\cos(m_2 \ln r) + i \sin(m_2 \ln r) \Big], \tag{3}$$

the stresses oscillate infinitely rapidly as r approaches the wedge tip if $m_2 \neq 0$. Such oscillatory behavior is well documented for interface cracks in bi-material systems (England, 1965; Rice and Sih, 1965). Knowles and Sternberg, (1983) showed that such oscillatory behavior arises from the linearization of the field equations; by carrying out asymptotic analysis of the nonlinear field equations governing an interface crack between two compressible neo-Hookean sheets, they found that the crack faces open smoothly, and the stress field has no oscillatory behavior.

Figure 2 plots the numerical solution of (2) against θ_0 for v=0.33, 0.45 and 0.5 (incompressible solid). For the case of v=0.5, m is real for all angles. However, this is not the case for v<0.5, where complex root can exist. Note that Re m versus θ_0 has a cusp at some m, to the left of this cusp, m is real while m is complex to its right. The solid black line in Fig. 2 is the result of the finite strain theory (details are given in section 3 – 4). In finite strain theory there are no complex roots and stresses has no power singularity for $\theta \le \pi/2$ (see below for details).

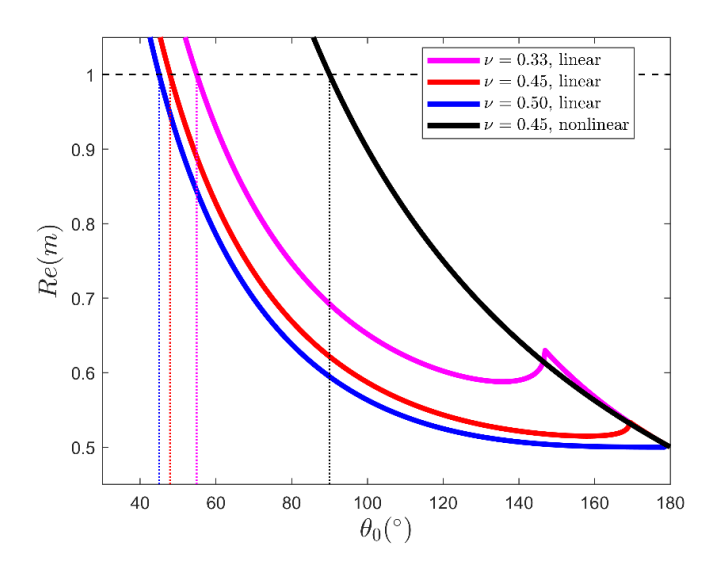


Figure 2: The real part of the singularity index m in the linear theory for v = 0.3, 0.45 and 0.5.

We highlight the following results of the linear theory for comparison purposes:

- The stress field has a power singularity and is unbounded if $\operatorname{Re} m < 1$. It is bounded when $\operatorname{Re} m \ge 1$.
- For an incompressible solid loaded in plane strain, m is always real and m=1 at $\theta_0 = \pi/4$ or 45 degrees. Thus, the stress and strain fields are bounded and continuous when $\theta_0 \le \pi/4$. Note that this is consistent with the result of Aksak et al. (Aksak, Sahin and Sitti, 2014), suggesting that the optimal pull-off force occurs when the singular fields near the wedge tip is eliminated.
- For compressible solids, m is complex for wedge angles, $\theta_0 > \theta_c(\nu)$, where $\theta_c(\nu)$ denotes the critical angle where the transition from real to complex root occurs. A plot of $\theta_c(\nu)$ versus ν is given in the SI. For wedge angles greater than $\theta_c(\nu)$, the stress field is singular and oscillates infinitely rapidly at the tip. We shall see later that this oscillatory behavior is absent in large deformation.
- For $\theta_0 = \pi/2$, $m = m_1 < 1$ for all $\nu > 0$, hence the stress has a non-oscillatory singularity r^{m-1} . As shown in Figure 3, the singularity index is found to decrease with increasing ν ; hence the stress is most singular when $\nu = 1/2$. We shall see later that the large deformation solution does not admit a power law singularity when $\theta_0 = \pi/2$. Instead, a much weaker logarithmic singularity is found for this case.

A brief discussion of transition between the linear and nonlinear asymptotic solutions are given in the SI.

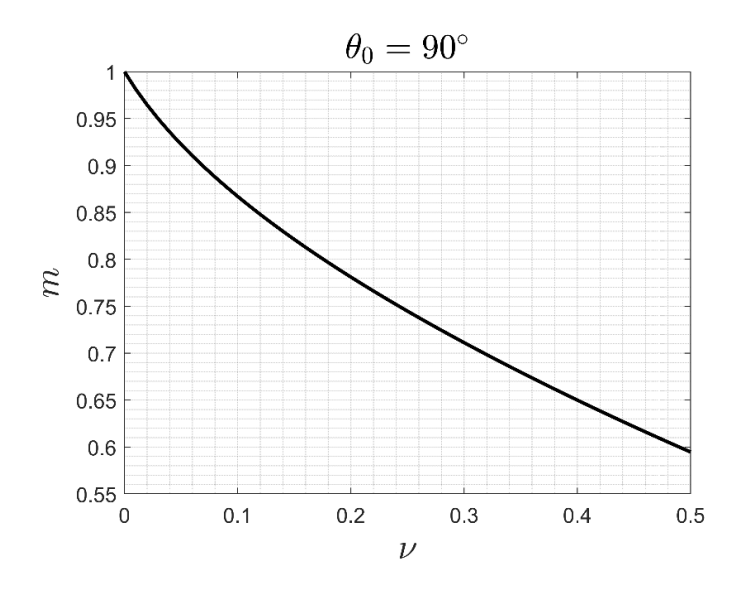


Figure 3: The singularity index for $\theta_0 = \pi/2$ as a function of the Poisson's ratio v. For this angle m is always real and less than I except at v=0, indicating that the stress has power singularity of the form $r^{\lambda-1}$ for v>0.

3. Finite strain model of wedge tip fields

3.1 Problem formulation and geometry

The geometry consists of a compressible hyper-elastic wedge of angle θ_0 bonded to the surface of a rigid substrate (see Figure 1). A material point in the reference undeformed configuration is denoted by its Cartesian coordinates x_i (i = 1,2,3). We consider plane strain deformation where all field quantities are independent of the out of plane coordinate x_3 . In the following we will use Greek indices to denote in plane coordinates, e.g., x_{α} , $\alpha = 1,2$. Details on plane strain deformation were given by Stephenson (Stephenson, 1982). Here we summarize the basic equations.

In plane strain, the out of plane deformation is exactly zero, so deformation can be represented by a 2D deformation gradient tensor F with Cartesian components $F_{\alpha\omega} = \partial y_{\alpha} / \partial x_{\omega}$, where $y_{\alpha} = x_{\alpha} + u_{\alpha}(x_1, x_2)$ is the deformed coordinates of the material point and u_{α} is its displacement in the α direction. The strain energy density function W for an isotropic hyper-elastic solid undergoing plane strain deformation is a function of two invariants $I = tr(FF^T)$ and $J = \det F$. The 1st Piola or nominal stress tensor P is related to W(I,J) by

$$\mathbf{P} = 2\frac{\partial W}{\partial I}\mathbf{F} + J\frac{\partial W}{\partial I}\mathbf{F}^{-T}.$$
 (4)

The true or Cauchy stress tensor τ is related to the 1st Piola stress tensor by

$$\boldsymbol{\tau} = J^{-1} \boldsymbol{P} \boldsymbol{F}^{T} \,. \tag{5}$$

3.2 Material Model

We consider a compressible hyper-elastic solid proposed by Blatz and Ko, (1962). As noted in the introduction, this material model was used by Lengyel et al., (Lengyel, Long and Schiavone, 2014) to study the asymptotic behavior of an interface crack between a compressible hyper-elastic solid and a rigid substrate ($\theta_0 = \pi$). The 2D plane strain energy density function is given by

$$W = \frac{\mu}{2} (I - 2) + \frac{\mu}{2\beta} (J^{-2\beta} - 1) \quad , \tag{6}$$

where μ is the small strain shear modulus. The dimensionless constant β is the compressibility factor, it is related to the small strain Poisson's ratio ν by $\beta = \nu/(1-2\nu) \ge 0$. This relation indicates that large β corresponds to low compressibility. For many soft materials, such as elastomers and gels, the resistance to shear is much smaller than the resistance to compression, resulting in $\beta >> 1$. For example, an elastomer used in many applications is Polydimethylsiloxane (PDMS). The Poisson's ratio of PDMS (Sylgard 184) was reported by Muller et al., (2019) to be 0.495, which corresponds to $\beta = 49.5$. The in-plane nominal stress tensor components $P_{\alpha\beta}$ are obtained using (4) and (6), they are

$$P_{11} = \mu \Big[F_{11} - J^{-2\beta - 1} F_{22} \Big], \qquad P_{12} = \mu \Big[F_{12} + J^{-2\beta - 1} F_{21} \Big]$$

$$P_{21} = \mu \Big[F_{21} + J^{-2\beta - 1} F_{12} \Big], \qquad P_{22} = \mu \Big[F_{22} - J^{-2\beta - 1} F_{11} \Big]$$
(7a-d)

The in-plane true stress components $\tau_{\alpha\omega}$ are evaluated using (7a-d) and (5), they are:

$$\begin{split} &\tau_{11} = J^{-1}\mu \Big\{ \Big[F_{11}^2 + F_{12}^2 \Big] - J^{-2\beta} \Big\} \\ &\tau_{12} = \tau_{21} = J^{-1}\mu \Big[F_{11}F_{21} + F_{12}F_{22} \Big] \\ &\tau_{22} = J^{-1}\mu \Big\{ \Big[F_{21}^2 + F_{22}^2 \Big] - J^{-2\beta} \Big\} \end{split} \tag{8a-d}$$

3.3 Equilibrium

In the absence of body forces², the equilibrium equations in the reference configuration are

$$\nabla_{\mathbf{x}} \bullet \mathbf{P} = \mathbf{0} \tag{9}$$

Substituting (7a-d) into (9), the equilibrium equations are:

$$\nabla_{x}^{2} y_{1} + (2\beta + 1) J^{-2(\beta+1)} (\nabla_{x} J \times \nabla_{x} y_{2}) \cdot E_{3} = 0$$

$$\nabla_{x}^{2} y_{2} - (2\beta + 1) J^{-2(\beta+1)} (\nabla_{x} J \times \nabla_{x} y_{1}) \cdot E_{3} = 0$$
(10a,b)

Where E_3 is the unit vector in the out of plane direction and ∇_x^2 is the 2D Laplacian in reference coordinates. As in section 2, we use the polar coordinates (r,θ) in the reference configuration as independent variables:

$$x_1 = r\cos\theta, \ x_2 = r\sin\theta \tag{11}$$

Using r,θ as independent variables, the equilibrium equations (10a,b) become:

$$\frac{1}{r}\frac{\partial}{\partial r}\left(r\frac{\partial u_{1}}{\partial r}\right) + \frac{1}{r^{2}}\frac{\partial^{2}u_{1}}{\partial\theta^{2}} + \frac{(2\beta+1)J^{-2(\beta+1)}}{r}\left[\frac{\partial J}{\partial r}\frac{\partial y_{2}}{\partial\theta} - \frac{\partial y_{2}}{\partial r}\frac{\partial J}{\partial\theta}\right] = 0$$

$$\frac{1}{r}\frac{\partial}{\partial r}\left(r\frac{\partial y_{2}}{\partial r}\right) + \frac{1}{r^{2}}\frac{\partial^{2}y_{2}}{\partial\theta^{2}} - \frac{(2\beta+1)J^{-2(\beta+1)}}{r}\left[\frac{\partial J}{\partial r}\left(-r\sin\theta + \frac{\partial u_{1}}{\partial\theta}\right) - \left(\cos\theta + \frac{\partial u_{1}}{\partial r}\right)\frac{\partial J}{\partial\theta}\right] = 0$$
(12a,b)

where J is

 $J = \frac{1}{r} \left[\left(\cos \theta + \frac{\partial u_1}{\partial r} \right) \frac{\partial y_2}{\partial \theta} - \frac{\partial y_2}{\partial r} \left(-r \sin \theta + \frac{\partial u_1}{\partial \theta} \right) \right]$ (12c)

These equations are the same as in Lengyel et al. (Lengyel, Long and Schiavone, 2014). However, it must be noted that Lengyel et al., (Lengyel, Long and Schiavone, 2014) used the symbol x_{α} to denote deformed coordinates. Also, instead of using y_1, y_2 as the dependent variables, which is typically adopted in nonlinear field analysis, we use u_1, y_2 as the dependent variables. Since $y_1 = u_1 + r \cos \theta$, the usage of u_1 as independent variable made the BC $y_1 = r$ on the interface homogeneous (see (13a) below).

² As long as the body forces are bounded, they have no effect on the leading singular behavior of the fields.

3.4 Boundary conditions (BC) for Asymptotic Analysis

We consider perfect bonding, hence the displacements on the interface $\theta = 0, r > 0$ are identically zero, i.e.,

$$u_1(\theta = 0, r > 0) = 0, \quad y_2(\theta = 0, r > 0) = 0$$
 (13a,b)

The edge of the wedge at $\theta = \theta_0, r > 0$ is traction free, i.e.,

$$\mathbf{P} \bullet \mathbf{N} = \mathbf{0} \tag{14}$$

where N is the unit normal vector to the free edge. Using (7a-d), the BC (14) can be written in terms of u_1, y_2 as:

$$-\sin\theta_{0} + \frac{1}{r}\frac{\partial u_{1}}{\partial \theta} + J^{-2\beta-1}\frac{\partial y_{2}}{\partial r} = 0 \quad \text{at } \theta = \theta_{0}$$

$$\frac{1}{r}\frac{\partial y_{2}}{\partial \theta} - J^{-2\beta-1}\left(\cos\theta_{0} + \frac{\partial u_{1}}{\partial r}\right) = 0 \quad \text{at } \theta = \theta_{0}$$
(15a,b)

4. Asymptotic analysis of wedge tip fields

4.1 Asymptotic Analysis

In this work we assume $\theta_0 < \pi$ since the crack case where $\theta_0 = \pi$ was solved by Lengyel et al., (Lengyel, Long and Schiavone, 2014). We consider the expansion near r = 0,

$$u_{1} = r^{m_{1}} v_{1}(\theta) + o(r^{m_{1}})$$

$$y_{2} = r^{m_{2}} v_{2}(\theta) + o(r^{m_{2}})$$

$$0 < m_{\alpha} < 1$$
(16a,b)

The condition $0 < m_{\alpha} < 1$ enforces continuity of displacements but allows for singular stresses and displacement gradients. Substituting (16a,b) into (12c), we found

$$J \sim \frac{1}{r} \left[\left(\cos \theta + m_1 r^{m_1 - 1} v_1 \right) r^{m_2} v_2' - m_2 r^{m_2 - 1} v_2 \left(-r \sin \theta + r^{m_1} v_1' \right) \right]$$

$$\sim r^{m_1 + m_2 - 2} \left[m_1 v_1 v_2' - m_2 v_2 v_1' \right]$$
(17)

Eq.(16a) implies that the Laplacian term in (12a) is

$$\nabla_x^2 u_1 \sim r^{m_1 - 2} \left(v_1'' + m_1^2 v_1 \right), \tag{18a}$$

while the 2nd term in (12a) (we will call this the *nonlinear* term) is

$$\frac{J^{-2(\beta+1)}}{r} \left[\frac{\partial J}{\partial r} \frac{\partial y_2}{\partial \theta} - \frac{\partial y_2}{\partial r} \frac{\partial J}{\partial \theta} \right] \sim r^{-2(\beta+1)(m_1+m_2-2)} r^{2m_2-2} r^{m_1-2} . \tag{18b}$$

Using (18a,b), the ratio of the nonlinear to the Laplace term is seen to vanish as r goes to zero, i.e.,

$$r^{-2(\beta+1)(m_1+m_2-2)}r^{2m_2-2} = r^{-2(\beta+1)(m_1-1)}r^{-2\beta(m_2-1)} \to 0,$$
(19)

where we have used $0 < m_{\alpha} < 1$. Hence the nonlinear term (18b) can be neglected and the leading order behavior of (12a) is determined by (18a), i.e.,

$$v_1'' + m_1^2 v_1 = 0. (20)$$

The solution of (20) that satisfies the BC (13a) is

$$v_1 = a_1 \sin(m_1 \theta), \tag{21}$$

where a_1 is an arbitrary constant. To satisfy the traction free boundary condition (15a), we note that the third term in (15a) is of order

$$J^{-2\beta-1}\frac{\partial y_2}{\partial r} \sim r^{-(2\beta+1)(m_1+m_2-2)}r^{m_2-1} = r^{-(2\beta+1)(m_1-1)}r^{-2\beta(m_2-1)}.$$
 (22)

Comparing the order of each term in (15a), we have

$$\underbrace{-\sin\theta_{0}}_{O(1)} + \frac{1}{r} \frac{\partial u_{1}}{\partial \theta} + \underbrace{J^{-2\beta-1} \frac{\partial y_{2}}{\partial r}}_{O(r^{m_{1}-1})} = 0 .$$
(23)

The dominant term in (23) is clearly $\frac{1}{r} \frac{\partial u_1}{\partial \theta}$, hence, to leading order, the BC (15a) becomes:

$$\left. \frac{\partial u_1}{\partial \theta} \right|_{\theta_0} = 0 \Rightarrow v_1'(\theta_0) = 0 \Rightarrow \cos(m_1 \theta_0) = 0 \Rightarrow m_1 = \frac{\pi}{2\theta_0}. \tag{24}$$

Equation (24) determines the singularity index for the horizontal displacement u_1 . Here we note the assumption that $m_1 < 1$ holds if and only if $\theta_0 > \pi/2$.

We next consider the leading order solution of (12b), the Laplacian term is

$$\nabla^2 y_2 \sim r^{m_2 - 2} \left(v_2'' + m_2^2 v_2 \right). \tag{25a}$$

The nonlinear term is:

$$\frac{J^{-2(\beta+1)}}{r} \left[\frac{\partial J}{\partial r} \left(-r \sin \theta + \frac{\partial u_1}{\partial \theta} \right) - \left(\cos \theta + \frac{\partial u_1}{\partial r} \right) \frac{\partial J}{\partial \theta} \right] \sim r^{-2(\beta+1)(m_1+m_2-2)} r^{2m_1-2} r^{m_2-2} , \qquad (25b)$$

which goes to zero in comparison with the Laplacian term. Therefore,

$$v_2'' + m_2^2 v_2 = 0 \Rightarrow v_2 = a_2 \sin m_2 \theta \tag{26}$$

where we have used the BC (13b). The same argument shows that the leading order behavior of (15b) is

$$\frac{\partial y_2}{\partial \theta} \sim 0$$
 at $\theta = \theta_0 \Rightarrow \cos(m_2 \theta_0) = 0$. (27)

Equation (27) implies that

$$m_2 = \frac{\pi}{2\theta_0} = m_1 \equiv m. \tag{28}$$

Thus, the singularity index for u_1 and y_2 is equal.

We need to recalculate J since the leading order term in (17), $[m_1v_1v_2' - m_2v_2v_1'] = m[v_1v_2' - v_2v_1']$ vanishes identically (see (21) and (26)). A simple calculation using ((17), upper equation) shows that

$$J \sim \frac{1}{r} \left[\left(\cos \theta + a_1 m r^{m-1} \sin m \theta \right) a_2 r^m m \cos m \theta - a_2 m r^{m-1} \sin m \theta \left(-r \sin \theta + a_1 m r^m \cos m \theta \right) \right]$$
$$= a_2 m r^{m-1} \cos \left[\left(1 - m \right) \theta \right]$$

(29)

Comparing (29) with (17) shows that the leading order behavior of J has changed because $[m_1v_1v_2'-m_2v_2v_1']$ vanishes, it is now r^{m-1} instead of r^{2m-2} . However, since m < 1, J is still unbounded as r goes to zero. Note J is non-zero inside and on the wedge boundaries since $\cos\left[\left(1-m\right)\theta\right]>0$ in $0 \le \theta \le \theta_0$. However, because $\left[m_1v_1v_2'-m_2v_2v_1'\right]$ vanishes identically, J is now of order r^{m-1} , so we need to check that the Laplacian terms in (12a,b) still dominate the nonlinear term. This is indeed the case since

$$\frac{J^{-2(\beta+1)}}{r} \left[\frac{\partial J}{\partial r} \frac{\partial y_2}{\partial \theta} - \frac{\partial y_2}{\partial r} \frac{\partial J}{\partial \theta} \right] \sim r^{-2(\beta+1)(m-1)} r^{m-1} r^{m-2} >> r^{m-2}, \tag{30a}$$

$$\frac{J^{-2(\beta+1)}}{r} \left[\frac{\partial J}{\partial r} \left(-r \sin \theta + \frac{\partial u_1}{\partial \theta} \right) - \left(\cos \theta + \frac{\partial u_1}{\partial r} \right) \frac{\partial J}{\partial \theta} \right] \sim r^{-2(\beta+1)(m-1)} r^{m-1} r^{m-2} >> r^{m-2} . \quad (30b)$$

Thus, (21), (26), (28) are still valid provide that the leading behavior of J is given by (29).

4.2 Higher order terms

Our result in previous section shows that, in contrast to the linear theory where m is a function of the Poisson's ratio (see (2)), the singularity index m in the leading order solution of the finite strain theory *does not depend on the compressibility factor* β (see (28)). We show here that the effect of compressibility is manifested in higher order terms in the asymptotic expansion (see (43) below). To see this, consider

$$u_{1} = a_{1}r^{m} \sin m\theta + r^{n_{1}}w_{1}(\theta) + o(r^{n_{1}})$$

$$y_{2} = a_{2}r^{m} \sin m\theta + r^{n_{2}}w_{2}(\theta) + o(r^{n_{2}})$$
where $n_{\alpha} \ge 1$ (31a,b)

Since the first terms in (31a,b) satisfy the Laplace equation exactly, we have

$$\nabla^{2} u_{1} \sim r^{n_{1}-2} \left(w_{1}'' + n_{1}^{2} w_{1} \right)$$

$$\nabla^{2} y_{2} \sim r^{n_{2}-2} \left(w_{2}'' + n_{2}^{2} w_{2} \right)$$
(32a,b)

The leading order of J is still given by (29), more precisely,

$$J = r^{m-1}a_2m\cos\left[\left(1-m\right)\theta\right] + o(r^{m-1}) \tag{33}$$

Using (33) and (31a,b), the leading order behavior of the nonlinear term in (12a) is

$$\frac{1}{r} \left[\frac{\partial J}{\partial r} \frac{\partial y_2}{\partial \theta} - \frac{\partial y_2}{\partial r} \frac{\partial J}{\partial \theta} \right] \sim m^2 (1 - m) a_2^2 r^{m-1} r^{m-2} \left(\cos m\theta \cos \left[(1 - m)\theta \right] + \sin m\theta \sin \left[(1 - m)\theta \right] \right)$$

$$= (m - 1) a_2^2 m^2 r^{m-1} r^{m-2} \cos \theta$$
(34)

Combining (34) and (33), the leading order behavior of the nonlinear term in (12a) is

$$J^{-2(\beta+1)} \frac{1}{r} \left[\frac{\partial J}{\partial r} \frac{\partial y_2}{\partial \theta} - \frac{\partial y_2}{\partial r} \frac{\partial J}{\partial \theta} \right] = O(r^{2(\beta+1)(1-m)} r^{m-1} r^{m-2}) = O(r^{2\beta(1-m)-1})$$
(35)

Let us first assume that $n_1 > 1$. If the nonlinear term is small in comparison with the Laplacian term as r goes to zero, then

$$n_1 - 2 < 2\beta(1-m) - 1 \Leftrightarrow n_1 < 1 + 2\beta(1-m)$$
. (36)

Since 1/2 < m < 1, for any fixed $\theta_0 > \pi/2$ (36) is true for sufficiently large β . Let us assume this is the case since we are mostly interested in solids with low compressibility, then the Laplacian term dominates which results in

$$w_1'' + n_1^2 w_1 = 0 \Rightarrow w_1 = b_1 \sin(n_1 \theta). \tag{37}$$

Let us consider the boundary condition (15a). By (24), the term $\frac{1}{r} \frac{\partial u_1}{\partial \theta}$ in (15a) is of order $r^{n_1-1}w_1'$. However, it is impossible for this term to dominant (unless $\sin \theta_0 = \sin \pi = 0$, recall we exclude the crack case) since $n_1 > 1$ and this term vanishes as r goes to zero. The last term in the BC (15a) is

$$J^{-2\beta-1}\frac{\partial y_2}{\partial r} \sim r^{(2\beta+1)(1-m)}r^{m-1} = r^{(2\beta)(1-m)},\tag{38}$$

which also goes to zero as r goes to zero since m < 1. By (36) this term is small compared with $\frac{1}{r} \frac{\partial u_1}{\partial \theta} \sim \frac{r^{n_1}}{r} w_1'$ as r goes to zero. Thus, the 1st term in the BC (15a) dominates and the BC (15a) cannot be satisfied. This means that it is not possible for $n_1 > 1$. The only choice is $n_1 = 1$. For this case (36) is always satisfied since m is less than 1, so the Laplacian term dominates and (32a) and (13b) implies that

$$w_1 = b_1 \sin \theta . ag{39}$$

What about the BC (15a)? Using (38), the order of each term in (15a) is:

$$-\sin\theta_0 + b_1\cos\theta_0 + \underbrace{J^{-2\beta-1}\frac{\partial y_2}{\partial r}}_{r^{2\beta(1-m)}\to 0} = 0 \Longrightarrow b_1 = \tan\theta_0.$$

$$\tag{40}$$

Hence the $2^{\rm nd}$ order solution for u_1 is $r \tan \theta_0 \sin \theta$, that is

$$u_1 = a_1 r^m \sin m\theta + r \tan \theta_0 \sin \theta + o(r). \tag{41}$$

Having determine the next order term for u_1 , we turn to y_2 . Using (29), the first order behavior of the nonlinear term in (12b) is:

$$\frac{J^{-2(\beta+1)}}{r} \left[\frac{\partial J}{\partial r} \left(-r \sin \theta + \frac{\partial u_1}{\partial \theta} \right) - \left(\cos \theta + \frac{\partial u_1}{\partial r} \right) \frac{\partial J}{\partial \theta} \right]
\sim r^{2(\beta+1)(1-m)} r^{2m-3} \left\{ a_2 m \cos \left[(1-m)\theta \right] \right\}^{-2(1+\beta)} a_1 a_2 (m-1) m^2 \cos \theta$$
(42)

Again, the Laplace term in (12b) is of order r^{n_2-2} , assuming it dominates (this requires β to be sufficiently large, exactly how large we shall see below), we must have

$$r^{n_2-2} >> r^{2(\beta+1)(1-m)}r^{2m-3} \Rightarrow n_2 < 2\beta(1-m)+1$$
 (43)

Equation (43) implies that the linear term of the boundary condition (15b) is the dominant term, so:

$$\frac{1}{r}\frac{\partial y_2}{\partial \theta} \sim 0 \quad \text{at } \theta = \theta_0 \quad \text{and} \quad y_2(\theta = 0) = 0$$
 (44)

Since $n_2 \ge 1$, the solution of the Laplacian (32b) is

$$b_2 r^{n_2} \sin n_2 \theta \,, \quad n_2 = \frac{3\pi}{2\theta_0} \tag{45}$$

Thus,

$$y_2 = a_2 r^m \sin m\theta + b_2 r^{n_2} \sin n_2 \theta + o(r^{n_2})$$
(46)

To summarize, the asymptotic expansion of the deformed coordinates are:

$$y_1 = a_1 r^m \sin m\theta + r (\tan \theta_0 \sin \theta + \cos \theta) + o(r)$$

$$y_2 = a_2 r^m \sin m\theta + b_2 r^{n_2} \sin n_2\theta + o(r^{n_2})$$
 (47a-c)

$$m = \frac{\pi}{2\theta_0}, \qquad \pi/2 < \theta_0 < \pi$$

Equation (47a) shows that the $2^{\rm nd}$ order term of y_1 is given by $r(\tan\theta_0\sin\theta + \cos\theta)$ instead of $r\cos\theta$. Since J depends on the combination of leading and $2^{\rm nd}$ order terms of y_1 , we need to reevaluate J using (47a,b). A straightforward calculation using (47a,b) shows that the leading order behavior of J is

$$J \sim ma_2 r^{m-1} \frac{\cos\left(\theta_0 - (1 - m)\theta\right)}{\cos\left(\theta_0\right)} \equiv ma_2 r^{m-1} j(\theta) \quad m = \frac{\pi}{2\theta_0}$$

$$\tag{48}$$

Note that *J* has the *same power law* singularity as in (33). However, although it is positive everywhere for $0 \le \theta < \theta_0$, it vanishes at θ_0 since $m = \frac{\pi}{2\theta_0}$. The vanishing of *J* on the

free edge implies that there is a boundary layer at $\theta = \theta_0$. The vanishing of J is important, because the traction free BC (24) and (27) relies on the assumption that the boundary terms associated with J were subdominant. This assumption is questionable if the asymptotic behavior of J at $\theta = \theta_0$ were unknown. The same issue was faced by Lenyel et al., (Lengyel, Long and Schiavone, 2014), who derived the near-tip fields for the special case of an interface crack where $\theta_0 = \pi$. In their work, they also found J vanishes at the crack face. They showed that J does not vanish at $\theta = \pi$ but has a different asymptotic behavior as $r \to 0$. Following the same line of reasoning (see Supporting information (SI)), we found a similar result where

$$J(r \to 0, \theta = \theta_0) = O(r^{-(1-m)/(1+\beta)})$$
 (49)

Substituting (49) into the traction free BC confirms that (24) and (27) is still valid, hence our leading order solution given by (47a,b) is still valid for all $\beta > 0$. However, the higher order terms in (47a,b) are only valid away from the boundary layer near the free edge. This claim is verified by the FE solution below.

4.3 Stresses

Using (47a,b), the components of the deformation gradient tensor, to leading order are

$$F_{11} = a_1 m r^{m-1} \sin[(m-1)\theta], F_{12} = a_1 m r^{m-1} \cos[(m-1)\theta]$$

$$F_{21} = a_2 m r^{m-1} \sin[(m-1)\theta] F_{22} = a_2 m r^{m-1} \cos[(m-1)\theta]$$
(50a-d)

The leading asymptotic behavior of the I^{st} *Piola stresses* can be evaluated using (7a-d) by ignoring the high order $J^{-2\beta-1}$ term and using (50a-d), this results in

$$P_{11} = \mu a_1 m r^{m-1} \sin \left[(m-1)\theta \right], \qquad P_{12} = \mu a_1 m r^{m-1} \cos \left[(m+1)\theta \right]$$

$$P_{21} = \mu a_2 m r^{m-1} \sin \left[(m+1)\theta \right], \qquad P_{22} = \mu a_2 m r^{m-1} \cos \left[(m-1)\theta \right]$$
(51a-d)

The leading behavior of the true stresses are found using (8a-d), these are:

$$\tau_{11} = \mu \frac{a_1^2 m r^{m-1}}{a_2 j(\theta)}
\tau_{12} = \tau_{21} = \mu a_1 m r^{m-1} / j(\theta),
\tau_{22} = \mu a_2 m r^{m-1} / j(\theta)$$
(52a-c)

where $j(\theta)$ is defined by (48). Note angular variation of true stress is *identical for different stress components*. In particular, all stress components have the same power law singularity at the wedge tip, reflecting the mixed mode nature of the local fields. Analogous to stress intensity factors in fracture mechanics, the parameters a_1, a_2 uniquely characterize the strength of the singularity near the wedge tip. Equations (52a-c) imply that the ratio of different true stress components are *constants independent* of r and θ . Specifically,

$$\tau_{12} / \tau_{11} = \tau_{22} / \tau_{12} = a_2 / a_1. \tag{53}$$

The ratio a_2/a_1 measures the ratio of interfacial shear stress to the transverse stress (τ_{11}) or the ratio of the normal stress to the shear stress respectively. In analogy to interfacial fracture mechanics, we define a phase angle ϕ_p

$$\phi_p = \tan^{-1}(a_2 / a_1) = \tan^{-1}(\tau_{12} / \tau_{11}) = \tan^{-1}(\tau_{22} / \tau_{12}). \tag{54a}$$

Equations (47a,b) provide another interpretation of phase angle, that is,

$$\lim_{r \to 0, \theta = \theta_0} (y_2 / y_1) = a_2 / a_1$$
(54b)

Equation (54b) shows that the free edge of the wedge near the tip deforms into a straight line with slope given by the phase angle ϕ_p . It is important to note that the intensity factors a_{α} cannot be determined by asymptotic analysis since they depend on the manner of loading and specimen geometry. Therefore, the local slope of the deformed wedge depends on the applied load and the specimen geometry.

4.4 Deformed shape of the free edge

The asymptotic behavior (47a,b) states that at the free edge

$$y_1 \sim a_1 r^m - c(\theta_0) r$$
 $c(\theta_0) \equiv -(\tan \theta_0 \sin \theta_0 + \cos \theta_0) = -\sec \theta_0 > 0$ (55a)

$$y_2 \sim a_2 r^m \tag{55b}$$

Thus, the deformed free surface is locally described by the equation

$$y_1 = \frac{a_1}{a_2} y_2 - c(\theta_0) (y_2 / a_2)^{1/m}$$
 (55c)

The location of the maximum of y_1 is found by solving $dy_1/dy_2 = 0$, i.e.,

$$\frac{a_1}{a_2} = \frac{c(\theta_0)}{m} (y_2 / a_2)^{1/m} y_2^{-1} \Rightarrow y_2 = [a_1 m \cos \theta_0]^{\frac{m}{1-m}} a_2$$
 (55d)

4.5 More higher order terms: William's expansion for nonlinear fields $(\pi \ge \theta_0 > \pi/2)$

Depending on β , we can generate additional higher order terms and obtain a William's type of expansion for nonlinear fields for wedge angle greater than 90 degrees. Let

$$u_{1} = a_{1}r^{m} \sin m\theta + r \tan \theta_{0} \sin \theta + r^{m_{12}}v_{12}(\theta) + o(r^{m_{12}})$$

$$y_{2} = a_{2}r^{m} \sin m\theta + a_{22}r^{m_{22}} \sin m\theta_{22}\theta + r^{m_{23}}v_{23}(\theta) + o(r^{m_{23}})$$
(56a,b)

where we have *modified notations* in (39a,b) so $b_2 = a_{22}$ and $m_{22} = n_2 = 3\pi/2\theta_0$. Also, $m_{12} > 1$ and $m_{23} \ge m_{22} = 3\pi/2\theta_0$. Substituting (56a,b) and (53) into the BC (15a) shows that

$$v_{12}'(\theta_0) = 0 \tag{57a}$$

provide that

$$m_{12} < 2\beta(1-m)+1.$$
 (57b)

Then it is easy to verify that the Laplacian term in (12a) is, to leading order

$$\nabla^2 u_1 \sim r^{m_{12}-2} \left(v_{12}'' + m_{12}^2 v_{12} \right) \tag{58}$$

and is asymptotic dominant compared with the nonlinear term provided that (57b) is satisfied.

Equations (58) and (57a) and (13a) imply that

$$v_{12} = a_{12} \sin(m_{12}\theta) \quad m_{12} = 3\pi / (2\theta_0) \tag{59}$$

Thus, the higher order terms depend on the value of β . Since we are interested in almost incompressible solids, β is typically very large so the condition (57b)

$$2\beta(1-m) + 1 > m_{12} = 3\pi / (2\theta_0)$$
(60)

is easily satisfied. Following the same line of reasoning we can determine m_{23} and $v_{23}(\theta)$ in (56b),

Indeed, we can continue this process to any positive integer $N \ge 2$ provided that

$$m_{\alpha N} < 2(1-m)\beta + 1 \qquad \qquad \alpha = 1,2 \tag{61}$$

The result is:

$$u_{1} = a_{1}r^{m} \sin m\theta + r \tan \theta_{0} \sin \theta + \sum_{k=2}^{N} r^{m_{1k}} \sin(m_{1k}\theta) + o(r^{m_{1,N}})$$

$$y_{2} = a_{2}r^{m} \sin m\theta + \sum_{k=2}^{N} a_{2k}r^{m_{2k}} a_{2k} \sin(m_{2k}\theta) + o(r^{m_{2,N}})$$
(62a,b)

where

$$m_{2k} = m_{1k} = \frac{(2k-1)\pi}{2\theta_0}$$
 (62c)

Note the number of terms in the asymptotic series (57a,b) depend on β ; specifically, this dependence is given by the inequality:

$$\frac{(2N-1)\pi}{2\theta_0} < 2\beta(1-m)+1. \tag{62d}$$

It should be noted that, unlike the William's expansion, which is an infinite series that converges within some radius of convergence at the crack tip; (62a,b) are asymptotic series, hence convergence is not guarantee, so including more terms of the series do not always lead to better accuracy.

5. Finite Element Results

5.1 Finite Element (FE) Calculations

We use FE to check our asymptotic analyses. The geometry of the wedge structure and the FE model is shown in Fig. 4(a,b). Calculations are performed using ABAOUS 2019. The bulk is modeled as a compressible Blatz-Ko material with energy density function given by (6). Calculations are performed using $\beta = 4.5$ which corresponds to $\nu = 0.45$. Let L be any arbitrary length scale, the specimen has a rectangular cross-section with sides $10L \times 11L$. On the top edge (BC), a uniform vertical displacement Δ is imposed while the horizontal shear traction is set to zero. The loading is controlled by the nominal stretch ratio $\lambda = 1 + \frac{\Delta}{11L}$. On the line directly ahead of the wedge tip (OD), the vertical and horizontal displacements are set to zero to simulate perfect bonding with the rigid substrate. The wedge face AO is traction free. The sides AB and CD are free of shear traction and remain straight during deformation. Our choice of boundary conditions is similar to those used by Lenyel et al. (Lengyel, Long and Schiavone, 2014). This choice allows us to check our FE result against theirs for the special case of $\theta_0=\pi$ (interface crack). Following Lenyel et al. (Lengyel, Long and Schiavone, 2014), we use triangular elements for the entire mesh to prevent over-distortion of elements. Plane strain CPE6H elements are used. To balance the accuracy and efficiency of computation, we use a fine mesh near the wedge tip (the smallest element size is $\sim 1 \times 10^{-5} L$), while away from the tip the element size increases and is $\sim L/2$ near the top edge. Our convergence test shows that further refinement of the mesh does not affect the FE results.

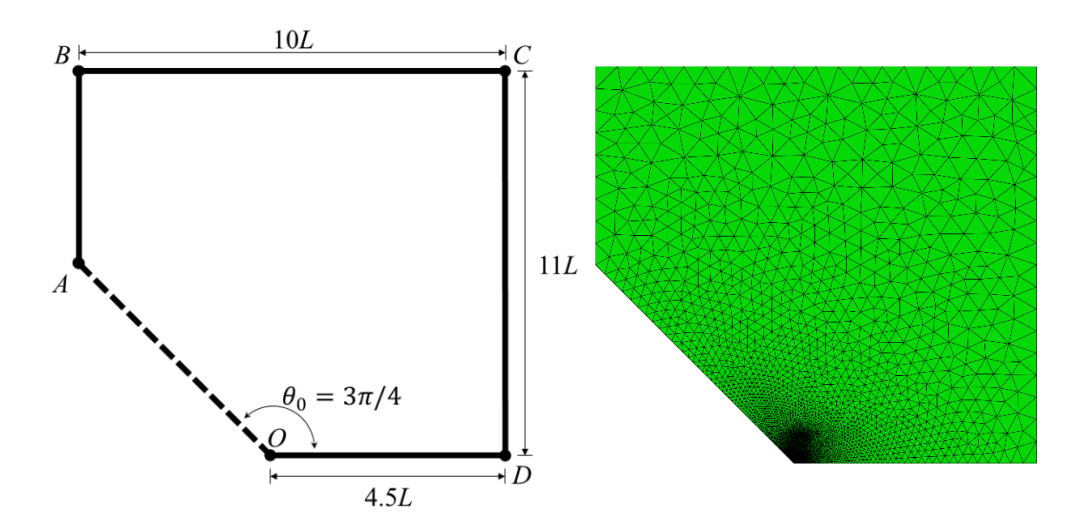


Figure 4 (a, left) Wedge geometry in undeformed reference configuration, (b, right) Mesh used in FE calculation. A uniform vertical displacement Δ is applied on the edge BC while the edge OD is fixed to the rigid substrate. On AB the shear traction is zero. The wedge face AO is traction free. The sides AB and CD are free of shear traction and remain straight during deformation (this removes the stress concentration at the corners at A and D). In this geometry, the only loading parameter is the nominal stretch ratio $\lambda \equiv 1 + \frac{\Delta}{11L}$.

5.2 Comparison of FE results with Asymptotic Theory

We carried out simulations for various obtuse wedges $\theta_0 > \pi/2$ and for $\beta = 4.5$. Here we present results for $\theta_0 = 3\pi/4 = 135^{\circ}$. FE results for other values of θ_0 also validate our asymptotic results and are given in the S3. Figure 5 shows that true stresses on the interface $(\theta = 0)$ versus distance from the wedge tip. The asymptotic results (52a-c) (solid lines with slope -1/3 in a log-log plot) are also plotted for comparison. The FE and asymptotic results are in good agreement for $r/L < 10^{-3}$.

To check the angular dependence of the true stresses we plot normalized FE true stress components $\overline{\tau}_{\alpha\beta} \equiv \tau_{\alpha\beta} \left(r/L = 10^{-3}, \theta\right)/\tau_{\alpha\beta} \left(r/L = 10^{-3}, \theta = 0\right)$ in Fig.6. If our asymptotic results (52a-c) are correct, then different components of $\overline{\tau}_{\alpha\beta}$ should coincide with $1/j(\theta)$. Figure 6 shows that this is indeed the case except for a boundary layer at θ_0 where $j(\theta_0) = 0$. As noted earlier, the existence of this boundary layer is expected (see discussion right after (48)). The deformed shape of the free edge obtained from FE is shown in Figure 7. Plotted in the same figure is the asymptotic result (55c). Again, there is good agreement between theory and FE results.

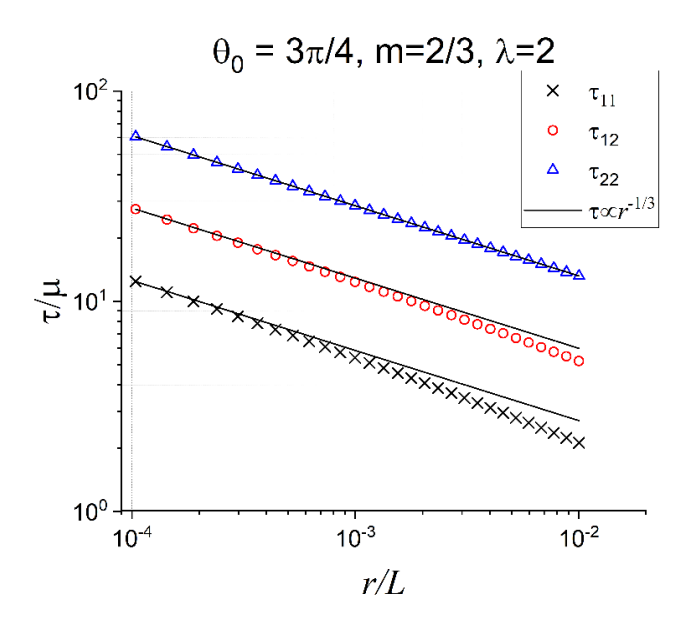


Figure 5 Normalized true stresses on the interface $(\theta = 0)$ for a 135 degrees wedge. Symbols are FE result, and the solid lines are the asymptotic results predicted by (52a-c).

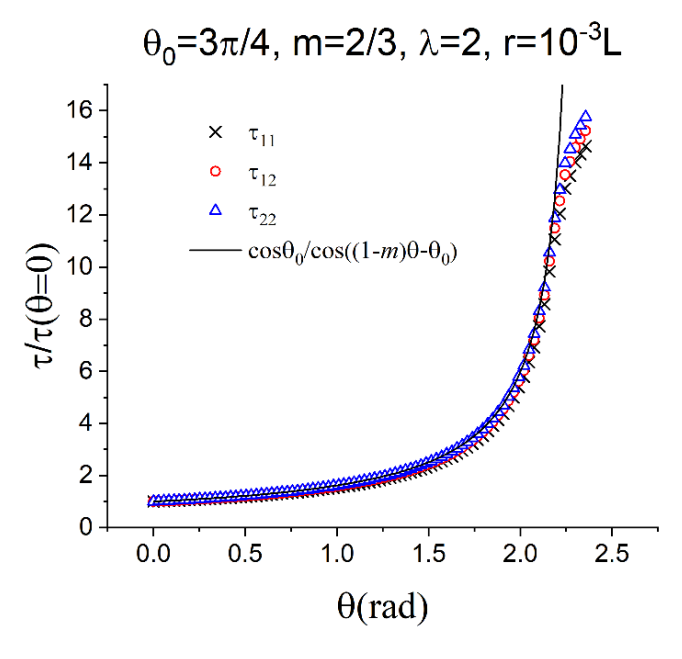


Figure 6 Different components of the normalized true stress versus θ . Prediction of the asymptotic results given by (52a-c) are the solid lines.

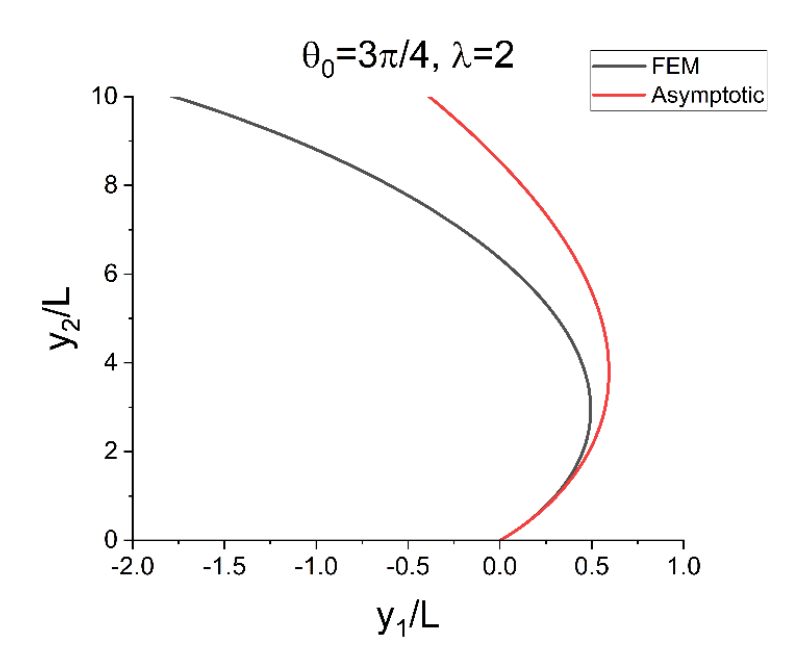
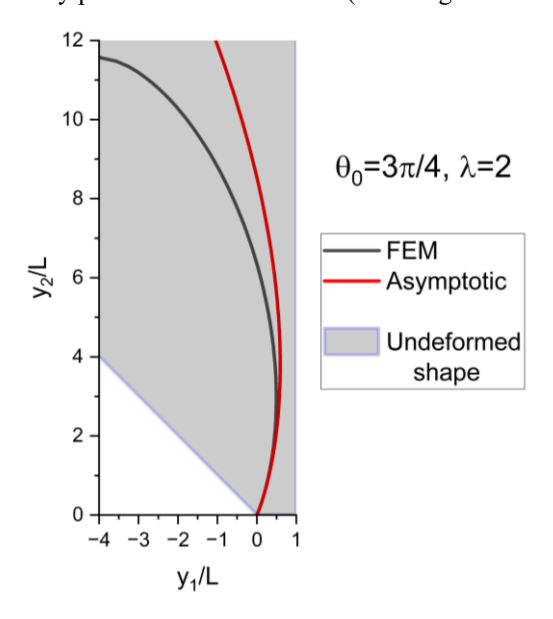


Figure 7 Deformed shape of the free edge. Black solid line is the FE result and red solid line is the asymptotic result (50c). The undeformed wedge surface (with angle $\theta_0 = 3\pi/4$) is the dotted line. Only part of the solid material (to the right of the deformed shape) is shown in figure.



6. Special Case: 90 Degrees Wedge

6.1 Shallow wedges: $0 < \theta_0 \le \pi / 2$

We call wedges with angles less than or equal to 90 degrees shallow wedges. For these wedges, our analysis indicates that the stresses cannot have a power singularity. Of course, this result does not prevent the stresses having a weaker singularity (e.g., a logarithmic singularity in r). Here we focus on the border-line case where $\theta_0 = \pi/2$.

This case appears often in applications, since many structures have 90° corners. Another reason to study this case is that we expect wedges with angles smaller than 90° will have weaker singularities, if they exist at all.

6.2 Results for 90 degrees wedge

The structure of the asymptotic fields near the corner turns out to be very difficult to analyze and we have not been able to obtain exact results. For this reason, we first present FE results. These FE results provide valuable insight on the near wedge tip fields. Based on these results, we obtain approximate close form expressions for the true stresses near the wedge tip. The FE geometry is a square with sides 10L. The boundary conditions are the same as $\theta_0 > \pi/2$.

The normalized true stresses $\tau_{\alpha\omega}/\mu$ along the interface $(\theta=0)$ versus distance r from the wedge tip for two different applied stretch ratios $\lambda=1.5,5.0$ are plotted in Fig. 8a, b. As shown in Fig. 8a, b, these FE results (symbols) of near tip stress components can be well approximated by

$$\tau_{11} / \mu = B_1 (\ln r)^2 + C_1 \ln r + D_1$$

$$\tau_{12} / \mu = C_2 \ln r + D_2$$

$$\tau_{22} / \mu = D_3$$
(63a-c)

The dimensionless parameters B_i, C_i and D_i in (63a-c) are functions of θ and the applied stretch ratio λ .

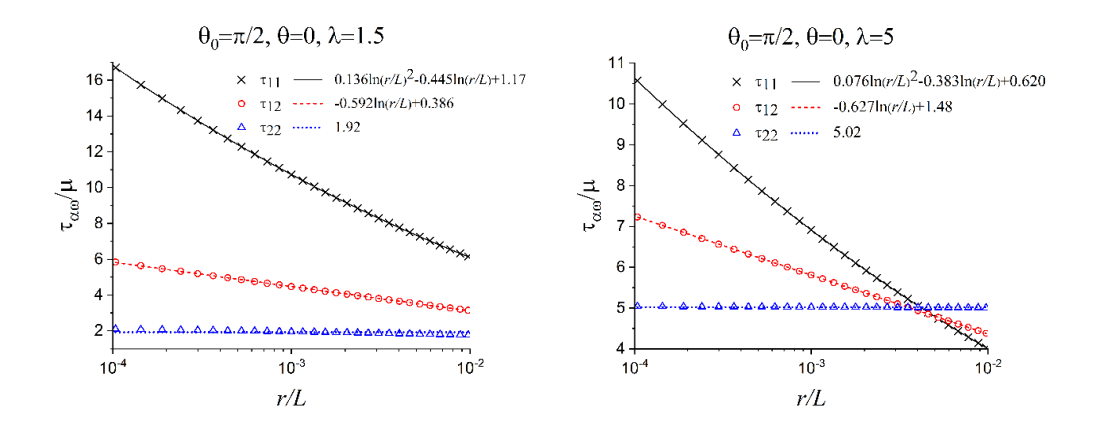
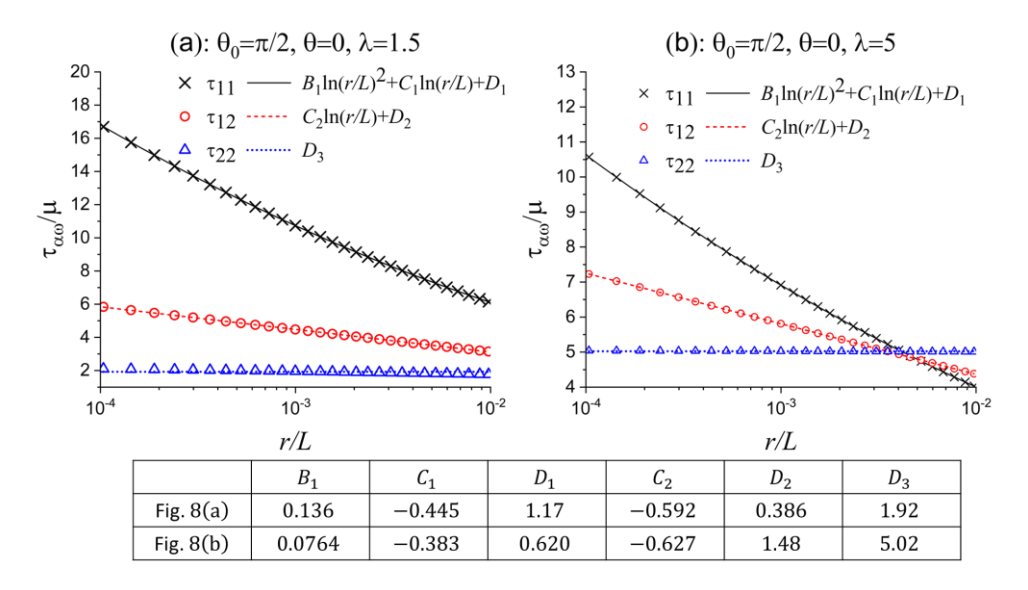


Fig. 8 True stress components directly ahead of wedge tip $(\theta = 0)$ for a 90 degrees wedge. Fig. 8a, (left), $\lambda = 1.5$, $\beta = 4.5$. Fig. 8b (right), $\lambda = 5$, $\beta = 4.5$. Symbols are FE results and solid lines are eq. (63a-c).



To study the angular variation of B_i, C_i, D_i we evaluate the true stresses on $\theta = \pi/2$. On this edge, the traction free condition implies that (see SI)

$$\tau_{11}\tau_{22} = \tau_{12}^2 \qquad \theta = \pi / 2 \tag{64}$$

We also confirmed (64) using our FE calculation. Equation (64) implies that B_i, C_i, D_i are not independent. Another way to see this is that stresses must satisfy equilibrium. Figures 9a,b plot the true stress along $\theta = \pi/2$ for two different applied stretches. The asymptotic results given by (63a-c) are plotted in the same figure as a comparison. Again, the agreement between FE and (63a-c) is excellent. These results strongly support the validity of (63a-c) for all angles. Results for true stress along $\theta = \pi/6, \pi/3$ are given in SI.

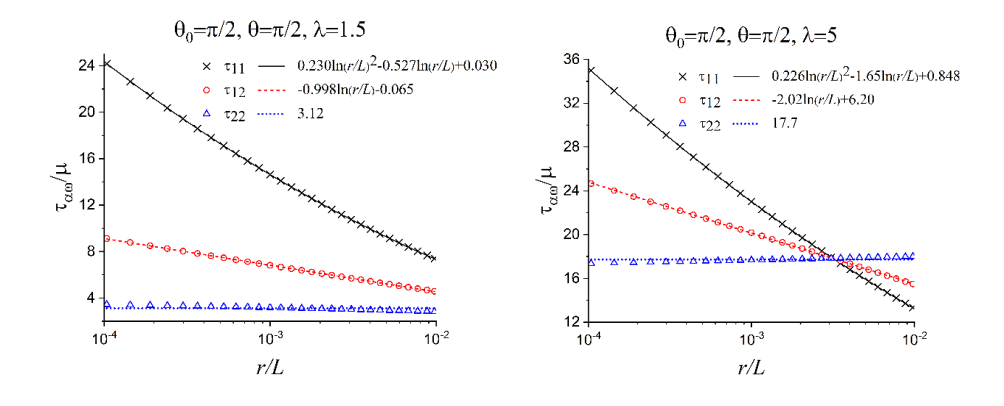
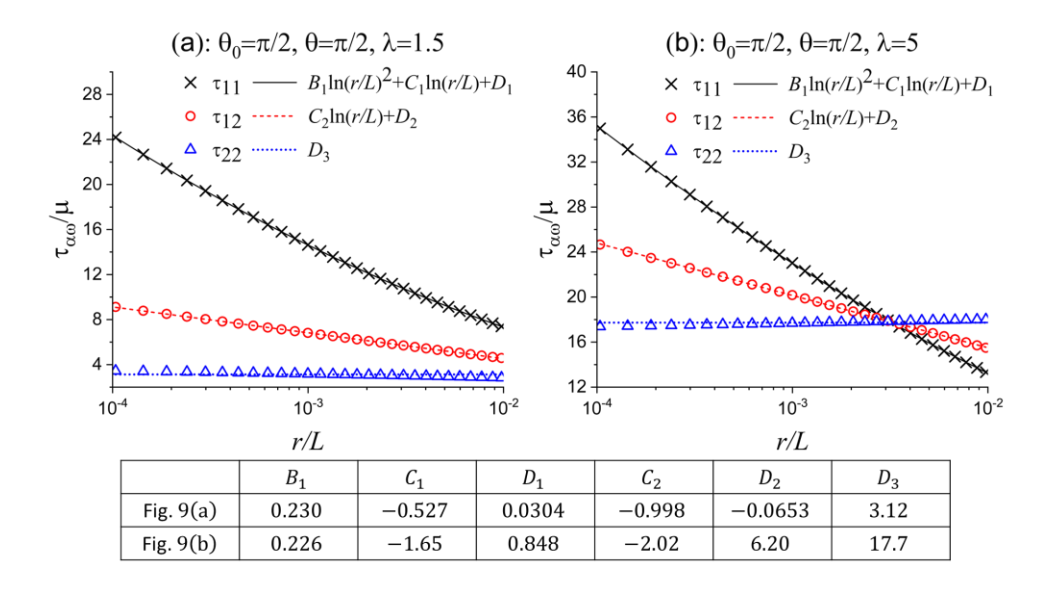


Fig.9 True stress distribution along the free edge for $\beta = 4.5$. $\lambda = 1.5$ (a, left). $\lambda = 5$ (b, right). Symbols are FE results and solid lines are eq. (63a-c).



The deformed shapes of the free edge are shown in Figure 10 for $\lambda = 1.5$, 2 and 5. It is interesting to note that the local wedge shape is not a monotonic function of the applied stretch. Up till $\lambda \approx 2$, the lateral surface contraction increases. This trend is reversed at large stretch ratio, e.g., $\lambda = 5$. This behavior is due to finite compressibility.

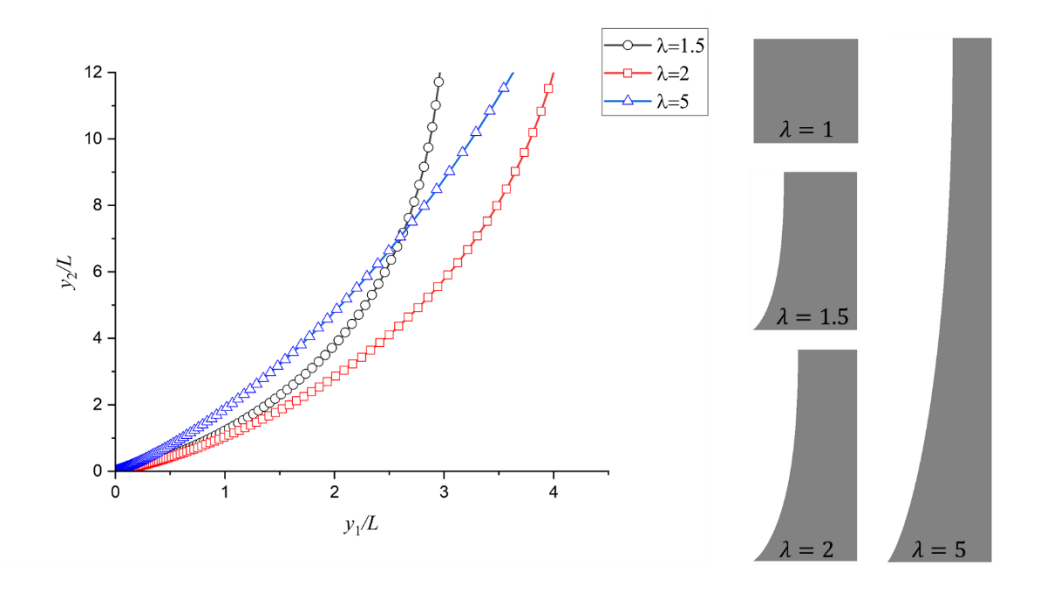


Fig. 10 Finite element results for the deformed shape of the free edge near the tip of a 90 degrees wedge for $\beta=4.5$. The applied stretch ratios are $\lambda=1.5$, 2.0 and 5.0. *Local* deformed shapes with origin at the wedge tip (left). Right figure shows the reference configuration $(\lambda=1)$ and the deformed shapes.

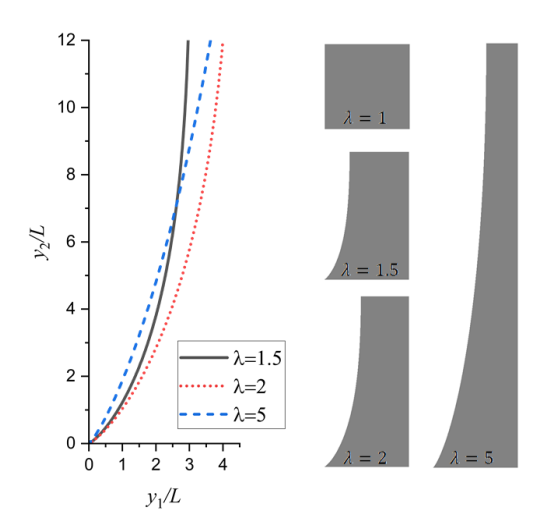


Figure.11 plots the asymptotic behavior of y_1 and y_2 on $\theta = \pi/2$, that is, the local deformed coordinates of the wedge surface. This figure shows that the expressions

$$y_{1} \sim A_{1}r\left[\left(\ln r\right)^{2}\right]^{\frac{\beta}{2\beta+1}},$$

$$y_{2} \sim A_{2}r\left[\left(\ln r\right)^{2}\right]^{\frac{\beta}{(2\beta+1)^{2}}},$$
(65a,b)

provide a good fit to the FE result. In (65a,b), A_1 and A_2 are dimensionless parameters that depend on λ and θ .

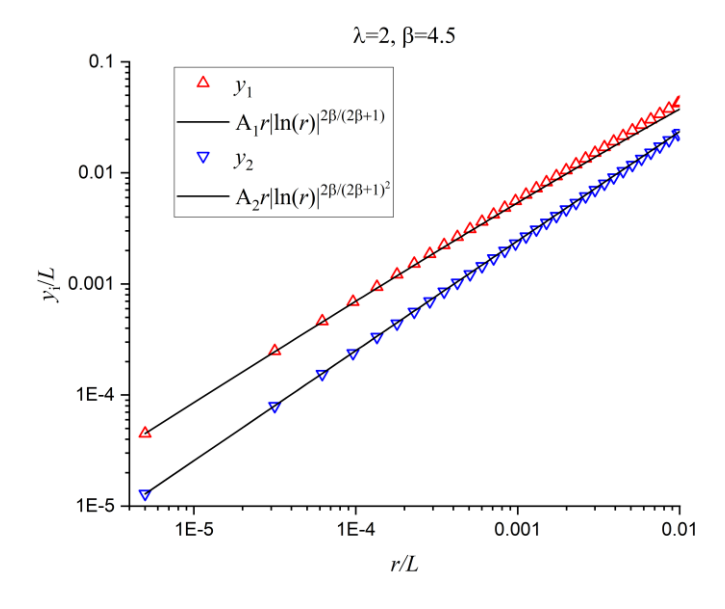


Figure.11 Deformed coordinates y_i (i = 1,2) versus normalized distance along the free edge ($\theta = \pi / 2$). The symbols are FE results, and the solid lines are the asymptotic expressions (65a,b).

Here we note that (65a,b) imply that

$$\frac{y_2}{y_1} \sim \frac{A_2}{A_1} \left[\left(\ln r \right)^{-2} \right]^{\frac{2\beta}{(2\beta+1)^2}} \tag{66}$$

Thus, the local slope vanishes at the wedge tip (recall that this local slope is always positive for an obtuse wedge).

A finite strain model based on a compressible Blatz-Ko model is used to study the plane

7. Summary and Discussion

strain deformation field near the tip of wedges with internal angles between $\theta_0 \in (0, \pi)$. For reentrant corners where $\theta_0 > \pi/2$, the true stresses (as well as the 1st Piola stress) as the wedge tip is approached have a power law singularity of the form r^{m-1} where $m = \frac{\pi}{2\theta}$. Our asymptotic analysis is confirmed by FE calculations. The magnitude of these wedge tip fields are controlled by two loading parameters, a_1 and a_2 , analogous to mixed mode stress intensity factors in linear elastic fracture mechanics. Specifically, the ratio a_2/a_1 measures the ratio of interfacial shear stress to the transverse stress (τ_{11}) or the ratio of the normal stress to the shear stress respectively. An interesting result is that the local deformed shape of the wedge is a straight line with slope determined by a_2 / a_1 . Hence, the wedge in the reference configuration is mapped to another wedge in the deformed configuration. A surprising result is that the leading asymptotic behavior is independent of the small strain Poisson's ratio or β , in contrast to small strain theory (see Fig. 2). Furthermore, for a given wedge angle $\theta_0 \in (\pi/2, \pi)$, the singularity index is larger than the singularity index predicted by the linear theory. As a result, the stress singularity predicted by the nonlinear theory is less severe. Note this is not always true, for example, for a Mode I crack in a homogenous neo-Hookean incompressible solid, the opening component of the true stress directly ahead of the crack tip has a higher singularity than that predicted by linear theory (Long and Hui, 2015). In addition, the singular stress fields in the nonlinear theory have no oscillation. This result is consistent with Knowles and Sternberg, (1983), who show that the stress field of an interface crack between two different neo-Hookean sheets does not have infinite oscillations. For sufficiently low compressibility or large β , we obtain higher order terms of the asymptotic series – analogous to William's expansion in linear theory.

In contrast to the linear theory, we find no power law singularity when $\theta_0 \in (\pi/4, \pi/2]$. Instead, we found a transition in asymptotic behavior at $\theta_0 = \pi/2$. For a 90-degree

wedge, numerical result shows that the power law singularity of the true stresses is replaced by a much weaker logarithmic singularity. Although we cannot provide a rigorous proof that no singularity exists for $\theta_0 < \pi/2$; such a singularity, if it exists, will be extremely weak for these angles. An interesting result is that the local deformed shape of the 90° wedge has zero slope (see (66)). These departures from LEFM offer important insights into the limitations of small strain theory; they lead to better understanding of soft material failure and can serve as a useful tool aiding the interpretation of experiments. For example, our theory indicates that design of fibril tip architecture based on linear elastic wedge theory is conservative which increases the safety factor and can lead to more reliable reusable adhesives.

There are obvious limitations to our theory. Our asymptotic result is for the Blatz-Ko model. A difficulty with large deformation theory is that asymptotic results are constitutive model dependent. This means that if we use a different compressible model, the asymptotic result will be different. Furthermore, there is no proof that the limit where $\beta \to \infty$ in our solution corresponds to a neo-Hookean *incompressible* solid.

Declaration of Competing Interest

The authors declare that they have no known competing financial interests or personal relationships that could have appeared to influence the work reported in this paper.

Acknowledgements

C.Y. Hui and B. Zhu are supported by the National Science Foundation under Grant No. CMMI-1903308.

Reference

Aksak, B., Sahin, K. and Sitti, M. (2014) "The optimal shape of elastomer mushroom-like fibers for high and robust adhesion," *Beilstein J. Nanotechnol*, 5, pp. 630–638. doi:10.3762/bjnano.5.74. Arzt, E., Gorb, S. and Spolenak, R. (2003) "From micro to nano contacts in biological attachment devices," *Proceedings of the National Academy of Sciences*, 100(19), pp. 10603–10606. doi:10.1073/PNAS.1534701100.

Blatz, P.J. and Ko, W.L. (1962) "Application of Finite Elastic Theory to the Deformation of Rubbery Materials," *Transactions of the Society of Rheology*, 6(1), pp. 223–252. doi:10.1122/1.548937.

del Campo, A., Greiner, C. and Arzt, E. (2007) "Contact Shape Controls Adhesion of Bioinspired Fibrillar Surfaces," *Langmuir*, 23(20), pp. 10235–10243. doi:10.1021/la7010502.

David B. Bogy (1968) "Edge-Bonded Dissimilar Orthogonal Elastic Wedges Under Normal and Shear Loading," *Journal of Applied Mechanics*, 35(3), pp. 460–466. doi:10.1115/1.3601236.

Dempsey, J.P. and Sinclair, G.B. (1979) "On the stress singularities in the plane elasticity of the composite wedge," *Journal of Elasticity*, 9(4), pp. 373–391. doi:10.1007/BF00044615.

Dunn, M.L. *et al.* (1997) "Fracture initiation at sharp notches under mode I, mode II, and mild mixed mode loading," *International Journal of Fracture*, 84, pp. 367–381.

doi:10.1023/A:1007346203407.

Dunn, M.L., Suwito, W. and Cunningham, S. (1997) "Fracture initiation at sharp notches: Correlation using critical stress intensities," *International Journal of Solids and Structures*, 34(29), pp. 3873–3883. doi:10.1016/S0020-7683(96)00236-3.

England, A.H. (1965) "A Crack Between Dissimilar Media," *Journal of Applied Mechanics*, 32(2), pp. 400–402. doi:10.1115/1.3625813.

Gao, Y.C. (1990) "Elastostatic crack tip behavior for a rubber-like material," *Theoretical and Applied Fracture Mechanics*, 14(3), pp. 219–231. doi:10.1016/0167-8442(90)90021-Q. Geubelle, P.H. and Knauss, W.G. (1994a) "Finite strains at the tip of a crack in a sheet of hyperelastic material: I. Homogeneous case," *Journal of Elasticity*, 35(1–3), pp. 61–98. doi:10.1007/BF00115539.

Geubelle, P.H. and Knauss, W.G. (1994b) "Finite strains at the tip of a crack in a sheet of hyperelastic material: II. Special bimaterial cases," *Journal of Elasticity*, 35(1–3), pp. 99–137. doi:10.1007/BF00115540.

Geubelle, P.H. and Knauss, W.G. (1994c) "Finite strains at the tip of a crack in a sheet of hyperelastic material: III. General bimaterial case," *Journal of Elasticity*, 35(1–3), pp. 139–174. doi:10.1007/BF00115541.

Gorb, S. *et al.* (2006) "Biomimetic mushroom-shaped fibrillar adhesive microstructure," *Journal of The Royal Society Interface*, 4(13), pp. 271–275. doi:10.1098/RSIF.2006.0164.

Hein, V.L. and Erdogan, F. (1971) "Stress Singularities in a Two-Material Wedge," *International Journal of Fracture Mechanics*, 7(3), pp. 317–330. doi:10.1007/BF00184307.

Jagota, A. and Hui, C.Y. (2011) "Adhesion, friction, and compliance of bio-mimetic and bio-inspired structured interfaces," *Materials Science and Engineering: R: Reports*, 72(12), pp. 253–292. doi:10.1016/J.MSER.2011.08.001.

Kim, S. and Sitti, M. (2006) "Biologically inspired polymer microfibers with spatulate tips as repeatable fibrillar adhesives," *Applied Physics Letters*, 89(26), p. 261911. doi:10.1063/1.2424442.

Knowles, J.K. and Sternberg, E. (1973) "An asymptotic finite-deformation analysis of the elastostatic field near the tip of a crack," *Journal of Elasticity*, 3(2), pp. 67–107. doi:10.1007/BF00045816.

Knowles, J.K. and Sternberg, E. (1974) "Finite-deformation analysis of the elastostatic field near the tip of a crack: Reconsideration and higher-order results," *Journal of Elasticity*, 4(3), pp. 201–233. doi:10.1007/BF00049265.

Knowles, J. K. and Sternberg, E. (1983) "Large deformations near a tip of an interface-crack between two Neo-Hookean sheets," *Journal of Elasticity*, 13(3), pp. 257–293. doi:10.1007/BF00042997.

Lengyel, T.H., Long, R. and Schiavone, P. (2014) "Effect of interfacial slippage on the near-tip fields of an interface crack between a soft elastomer and a rigid substrate," *Proceedings of the Royal Society A: Mathematical, Physical and Engineering Sciences*, 470(2170). doi:10.1098/rspa.2014.0497.

Long, R. and Hui, C.Y. (2015) "Crack tip fields in soft elastic solids subjected to large quasi-static deformation - A review," *Extreme Mechanics Letters*, 4, pp. 131–155. doi:10.1016/J.EML.2015.06.002.

Mansouri, K. *et al.* (2016) "Singular elastostatic fields near the notch vertex of a Mooney–Rivlin hyperelastic body," *International Journal of Solids and Structures*, 80, pp. 532–544. doi:10.1016/J.IJSOLSTR.2015.10.013.

Marques, E.A.S. and da Silva, L.F.M. (2008) "Joint Strength Optimization of Adhesively Bonded Patches," *The Journal of Adhesion*, 84(11), pp. 915–934. doi:10.1080/00218460802505275. Muskhelishvili, N.I. (1977) "Some Basic Problems of the Mathematical Theory of Elasticity," doi:10.1007/978-94-017-3034-1.

Ornes, S. (2013) "Mussels' sticky feet lead to applications," *Proceedings of the National Academy of Sciences*, 110(42), pp. 16697–16699. doi:10.1073/PNAS.1317104110.

Rice, J.R. and Sih, G.C. (1965) "Plane Problems of Cracks in Dissimilar Media," *Journal of Applied Mechanics*, 32(2), pp. 418–423. doi:10.1115/1.3625816.

Spuskanyuk, A. v. *et al.* (2008) "The effect of shape on the adhesion of fibrillar surfaces," *Acta Biomaterialia*, 4(6), pp. 1669–1676. doi:10.1016/J.ACTBIO.2008.05.026.

Stephenson, R.A. (1982) "The equilibrium field near the tip of a crack for finite plane strain of incompressible elastic materials," *Journal of Elasticity*, 12(1), pp. 65–99. doi:10.1007/BF00043706.

Tramacere, F. *et al.* (2014) "Structure and mechanical properties of Octopus vulgaris suckers," *Journal of The Royal Society Interface*, 11(91). doi:10.1098/RSIF.2013.0816.

Williams, M.L. (1952) "Stress Singularities Resulting From Various Boundary Conditions in Angular Corners of Plates in Extension," *Journal of Applied Mechanics*, 19(4), pp. 526–528. doi:10.1115/1.2791085.

Supporting Information:

S1. Plot of $\theta_c(v)$ versus v

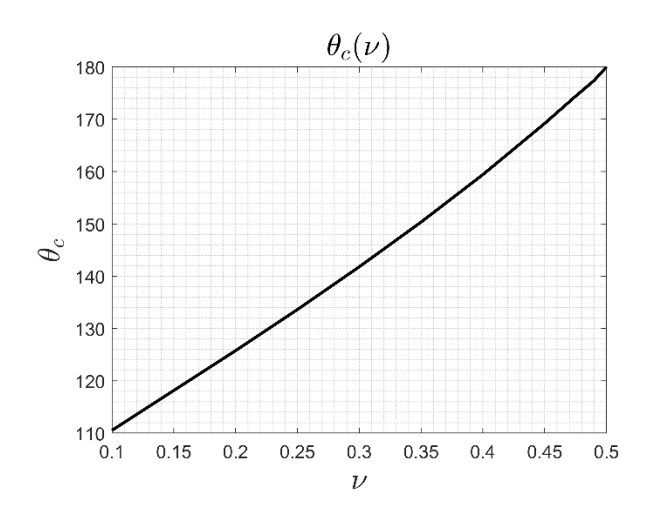


Figure S1: $\theta_c(v)$ versus v. Plot is generated by solving (2) and looking for first appearance of complex roots with real part between 0 and 1.

S2. Relation between asymptotic field of linear and nonlinear theory

Assume the applied load is so small so that there is a region where the linear corner field given by (1) dominates, i.e.,

$$\tau_{\alpha\omega} = A_1 r^{M-1} \hat{\tau}_{1\alpha\omega} (\theta, \theta_0, \nu) + A_2 r^{M-1} \hat{\tau}_{2\alpha\omega} (\theta, \theta_0, \nu)$$
 (S1)

Since the singularity index m for the linear and nonlinear problem is different; to avoid confusion, we replace m in the linear theory by M. Following the concept of small scale yielding in elastic-plastic fracture mechanics (Rice, 1966), we assume the region governed by nonlinear elasticity is so small in comparison with the size of the wedge, so the wedge can be replaced by a semi-infinite wedge in an infinite body and the actual boundary condition as $r \to \infty$ is given by (1). We call this the Small-Scale Nonlinear Elasticity (SSNE) problem. According to (52a-c), the near tip nonlinear stress fields are governed by two wedge intensity factors a_{α} , ($\alpha = 1, 2$). Here we present a scaling analysis to show how these stress intensities are related. In the following we assume that $\theta_0 > \pi/2$ so power singularity occurs for both linear and nonlinear theory, we also consider wedge angles that has no complex singularity index.

First, note that the stress intensity factors A_1, A_2 has the same dimension. Thus, the only length scale in the SSNE problem is:

$$\left(A_{\rm l}/\mu\right)^{1/(1-M)}\tag{S2}$$

This length scale is analogous to plastic zone size in elastic-plastic fracture. On the other hand, the nonlinear wedge intensities a_{α} have units of $(length)^{1-m}$ where m is given by (28). Dimensional analysis tells us that

$$a_{\alpha} = (A_{1} / \mu)^{(1-m)/(1-M)} \varphi_{\alpha} (\nu, \theta_{0}, A_{1} / A_{2})$$
 (S3)

where φ_{α} is a dimensionless function which must be determined by solving the full SSNE problem.

S3. Derivation of (49)

The following identity is useful for the study of asymptotic behavior of J: Equation 4 implies that

$$\boldsymbol{F}^{T}\boldsymbol{P} = 2\frac{\partial W}{\partial I}\boldsymbol{F}^{T}\boldsymbol{F} + J\frac{\partial W}{\partial J}\boldsymbol{I}$$
(S4)

Taking determinant of both sides, we have

$$\det \left[\mathbf{F}^{T} \mathbf{P} \right] = \det \mathbf{F}^{T} \det \mathbf{P} = J \det \mathbf{P} = \det \left[2 \frac{\partial W}{\partial I} \mathbf{F}^{T} \mathbf{F} + J \frac{\partial W}{\partial J} \mathbf{I} \right]$$
 (S5)

Next, use the fact that for 2D tensor, $\det[A + \lambda I] = \lambda^2 + \lambda t r A + \det A$. Applying this to (S5) with $\lambda = J \frac{\partial W}{\partial I}$, we have

$$J \det \mathbf{P} = \det \left[2 \frac{\partial W}{\partial I} \mathbf{F}^T \mathbf{F} + J \frac{\partial W}{\partial J} \mathbf{I} \right] = \left(J \frac{\partial W}{\partial J} \right)^2 + J \frac{\partial W}{\partial J} tr \left[2 \frac{\partial W}{\partial I} \mathbf{F}^T \mathbf{F} \right] + \det \left[2 \frac{\partial W}{\partial I} \mathbf{F}^T \mathbf{F} \right]$$

$$= \left(J \frac{\partial W}{\partial J} \right)^2 + 2 \frac{\partial W}{\partial I} J \frac{\partial W}{\partial J} tr \left[\mathbf{F}^T \mathbf{F} \right] + \left(2 \frac{\partial W}{\partial I} \right)^2 \det \left[\mathbf{F}^T \mathbf{F} \right]$$

$$= \left(J \frac{\partial W}{\partial J} \right)^2 + 2 \frac{\partial W}{\partial I} \frac{\partial W}{\partial J} IJ + \left(2 \frac{\partial W}{\partial I} \right)^2 J^2$$

(S6)

For our constitutive model, $2\frac{\partial W}{\partial I} = \mu$, $\frac{\partial W}{\partial J} = -\mu J^{-2\beta-1}$, hence (S6) is

$$\det \mathbf{P} = P_{11}P_{22} - P_{12}P_{21} = \frac{\left(\mu J^{-2\beta}\right)^2 - \mu^2 J^{-2\beta}I + \mu^2 J^2}{J} \tag{S7}$$

Thus

$$\left[\frac{P_{11}P_{22} - P_{12}P_{21}}{\mu^2}\right]J^{2\beta+1} = J^{-2\beta} - I + J^{2(\beta+1)}$$
(S8a)

where

$$I = F_{11}^2 + F_{21}^2 + F_{22}^2 + F_{12}^2. {(S8b)}$$

For obtuse wedges, the leading order behavior of I can be obtained using (50a-d), it is

$$I \sim m^2 \left(a_1^2 + a_2^2 \right) r^{-2(1-m)} \tag{S9}$$

Next, we note that the *BC* on the free edge implies that $\det \mathbf{P} = 0$ on the free edge, ((14) implies that the columns of \mathbf{P} are linear dependent). Hence (S7) implies that

$$J^{-4\beta-2} - J^{-2\beta-2}I + 1 = 0 \Leftrightarrow I = J^{2\beta+2} \left(1 - J^{-4\beta-2}\right) \theta = \theta_0$$
 (S10)

For obtuse wedges, I is unbounded as r goes to zero, this means that

$$I \sim J^{2\beta+2} \Rightarrow J = I^{1/(2\beta+2)} \qquad \theta = \theta_0 \tag{S11}$$

Substituting (S9) into (S11) give (49) in main text.

S4. FE results for $\theta_0 = 8\pi/9$ and $2\pi/3$: Comparison with Asymptotic result (52a-c)

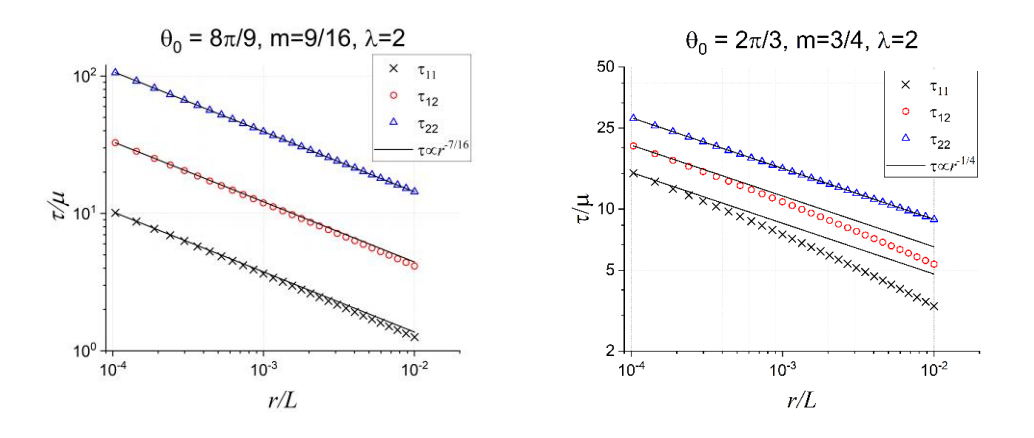


Fig. S2. Comparison of the asymptotic true stress component directly ahead of the wedge tip $(\theta = 0)$ (Eqn. (47a-c)) (solid lines) with FE results (symbols) for wedge angles:

$$\theta_0 = 8\pi / 9, 2\pi / 3$$

S5. Derivation of eq. 64

The traction free boundary on the free edge $\theta_0 = \pi/2$ implies that $P_{11} = P_{21} = 0$. Using $J\tau F^{-T} = P$ and enforcing this condition, with

$$J\mathbf{F}^{-T} = \begin{bmatrix} F_{22} & -F_{21} \\ -F_{12} & F_{11} \end{bmatrix} \Rightarrow \frac{\tau_{11}F_{22} - \tau_{12}F_{12} = 0}{\tau_{12}F_{22} - \tau_{22}F_{12} = 0}$$
(S12)

The last two equations imply eq. 64.

S6. True stress along $\theta = \pi / 6$ and $\pi / 3$ for **90** degrees wedge

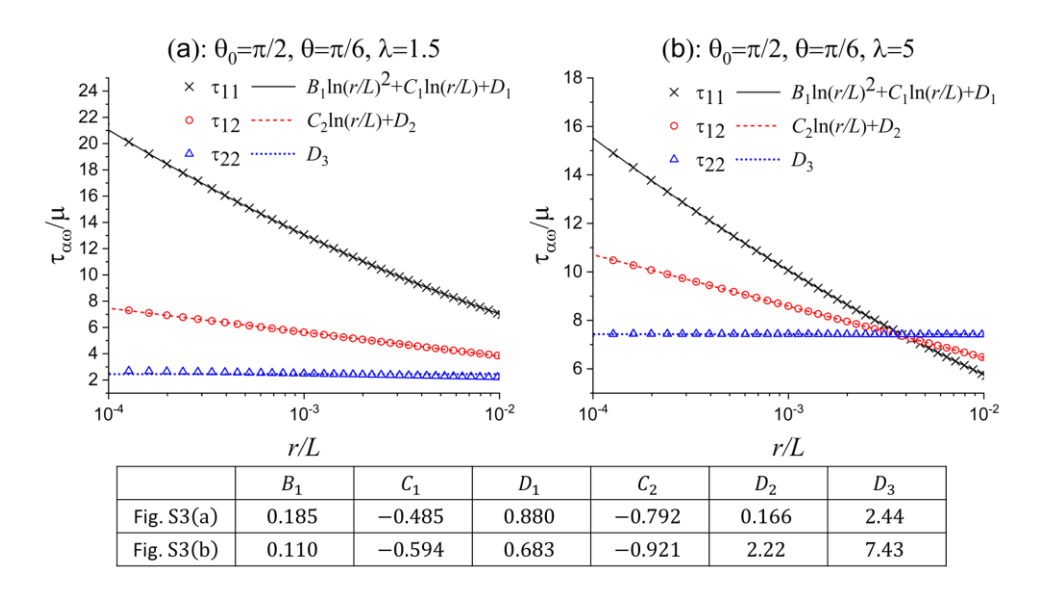


Fig.S3 True stress distribution along $\theta = \pi / 6$ for $\beta = 4.5$. $\lambda = 1.5$ (a, left). $\lambda = 5$ (b, right). Symbols are FE results and solid lines are eq. (63a-c).

Reference

Rice, J.R. Contained plastic deformation near cracks and notches under longitudinal shear. *International Journal of Fracture* **2**, 426–447 (1966). https://doi.org/10.1007/BF00183821